Modeling Methodology for a CMOS-MEMS Electrostatic Comb

Sitaraman Iyer[†], Hasnain Lakdawala[†], Tamal Mukherjee[†], and Gary K. Fedder[†*]
[†]Department of Electrical and Computer Engineering and [*]The Robotics Institute,
Carnegie Mellon University, Pittsburgh, PA 15213
Email: {sita, hasnain, tamal, fedder}@ece.cmu.edu

ABSTRACT

A methodology for combined modeling of capacitance and force in a multi-layer electrostatic comb is demonstrated in this paper. Conformal mapping-based analytical methods are limited to 2D symmetric cross-sections and cannot account for charge concentration effects at corners. Vertex capacitance can be higher than 30% of the total capacitance in a single-layer 2 μm thick comb with 10 μm overlap. Furthermore, analytical equations are strictly valid only for perfectly symmetrical finger positions. Fringing and corner effects are likely to be more significant in a multi-layered CMOS-MEMS comb because of the presence of more edges and vertices. Vertical curling of CMOS-MEMS comb fingers may also lead to reduced capacitance and vertical forces. Gyroscopes are particularly sensitive to such undesirable forces, which therefore, need to be well-quantified. In order to address the above issues, a hybrid approach of superposing linear regression models over a set of core analytical models is implemented. Design of experiments is used to obtain data for capacitance and force using a commercial 3D boundary-element solver. Since accurate force values require significantly higher mesh refinement than accurate capacitance, we use numerical derivatives of capacitance values to compute the forces. The model is formulated such that the capacitance and force models use the same regression coefficients. The comb model thus obtained, fits the numerical capacitance data to within 3%and force to within 10%.The model is experimentally verified by measuring capacitance change in a specially designed test structure. The capacitance model matches measurements to within 10%. The comb model is implemented in an Analog Hardware Description Language (AHDL) for use in behavioral simulation.
Keywords: electrostatic comb, force, capacitance, CMOS-MEMS, modeling

1 INTRODUCTION

Electrostatic combs are used extensively in MEMS for sensing and actuation. 1D and 2D analytical models for comb capacitance have been proposed. However, they all ignore the 3D vertex capacitance that can easily be at least 30% of the total capacitance in a comb as shown in Figure 1. Lateral combs with dominant motion along the length of the combs [1] (Figure 2) and differential combs with dominant motion along the direction of the gap [2] are the most common configurations. Lateral combs are used in microgyroscopes for actuation since they produce constant force over large amplitudes. Since microgyroscopes are highly sensitive to spurious forces, it is important to estimate the actuation forces produced by a lateral comb in all directions. Further, since temperature-dependent microstructure curling in CMOS-MEMS [4] gyroscopes can lead to drive amplitude drift over time, robust design requires curvature-inclusive comb actuator models. Simulation of manufacturing variations require models which are valid over a range of geometrical parameters. Lateral combs can also be used for sensing purposes, requiring an accurate capacitance model. Behavioral simulation can be used effectively to aid in gyroscope design only if the comb models provide reasonable estimates of capacitance and force. The modeling problem is particularly relevant in a CMOS-MEMS comb (Figure 3) which has multiple edges and vertices on each finger. In addition to providing accurate values for the capaci-

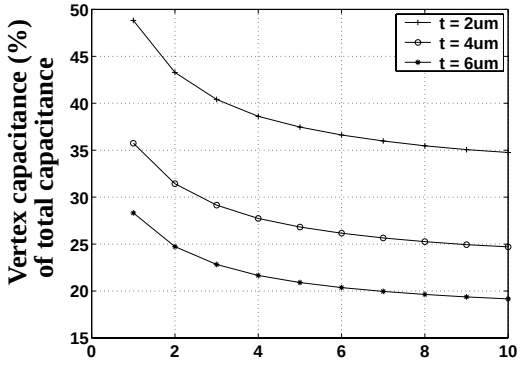

FIGURE 1. Significance of charge concentration at finger corners. The plot shows the percentage of total capacitance that is due to the finger corners for number of fingers ranging from 1 to 10 and finger thickness varying from 2 μm to 6 μm. The overlap of the fingers is kept constant at 10 μm. Note that for a 2 μm thickness, more than 30% of the total capacitance is due to the corners.

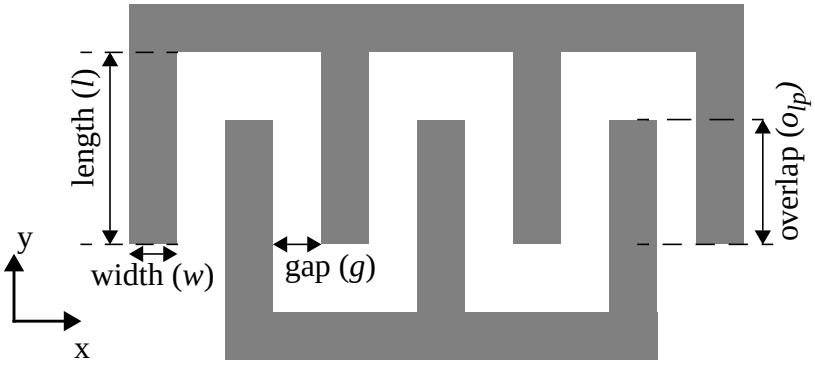

FIGURE 2. Top view of a lateral comb with three comb fingers (the lesser of the two numbers is taken as the number of fingers in the comb), with actuation force in the *y* direction. The cross-section of a typical finger is shown in Figure 3. The multi-layer cross-section leads to vertical curling of the comb fingers which is also included in the proposed comb model.

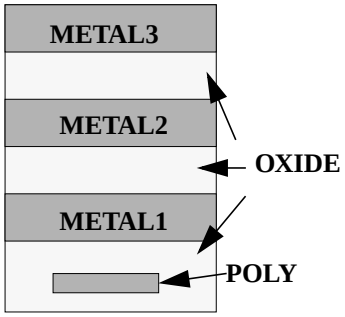

FIGURE 3. Cross-section of a comb finger in the CMOS-MEMS process

tance and a force, a behavioral model should also conserve energy [5].

Unlike elastic beam differential equations, which have a commonly valid closed-form general solution, the Laplace equation defining the electrostatic behavior of combs has closed form solutions only for a limited number of symmetrical boundary conditions, which are often restricted two dimensions. Most of the 2D analyses of the comb-drive cross-section use conformal mapping [6][7] techniques. These analyses are primarily aimed at the lateral comb with the dominant motion being in the direction of the length of the comb-fingers. Capacitance change due to vertical or lateral motion has been modeled using approximate analytical equations for single-layer comb fingers [7] or by numerical simulation of fixed-geometry 2D multi-layer cross-sections [8][9][10]. Angled comb-finger side-walls (observed in polysilicon microstructures) have been modeled by superposing curve-fits onto nominal analytical equations [11]. Change in fringe capacitance due to movement in the gap direction has not been considered in the any of the analytical models. Further, the analytical models described are strictly valid only under conditions of perfect symmetry and are not applicable for vertical or rotational motions which destroy the symmetry. None of the above-referred models take into account the fringe capacitance at the tips of the fingers, and the effect of the finger corners which can be significant as seen in Figure 1. While the numerical models [8][9][10] take into account the multi-layer nature of CMOS comb-drives (Figure 3), they are all valid only for fixed finger width and gap between the fingers. Further, because of the 2D nature of the models, capacitance changes and vertical forces due to temperature-dependent vertical curling of comb-fingers can only be approximated by assuming a mean vertical position of two uncurled combs.

Numerical methods such as Finite Element Analysis (FEA) and Boundary Element Analysis (BEA) can capture charge concentration, curling and generalized motion effects on capacitance and force. However, numerical convergence needs to be closely monitored. It has been our experience that even 4 times higher refinement of a boundary element mesh which yielded converged capacitance values did not yield converged force values. This is probably because capacitance convergence requires only that the overall charge on a conductor does not change with more refinement, however, force convergence imposes a much stricter condition that the charge distribution remains invariant with more refinement. Further numerical methods requiring meshed models and significant computation time, are not convenient for direct inclusion into a system simulation loop. Therefore, we choose as our modeling goal, a behavioral description of the comb which exhibits the ease of use of analytical equations in system-level simulation [12] while incorporating the extended validity range of numerical methods.

In [13] Gabbay et al. have presented a general macromodeling system, which employs a rational fraction of multivariate polynomial as the fitting equation. However, our proposed model consists of analytical equations at the core superposed with polynomial curve fits for data obtained from 3D BEA. The former approach is more suited (and probably necessary) for arbitrary shaped, non-parameterized geometry, deformable actuator systems. The electrostatic comb can be generally considered to be non-deformable (except for curvature, which is being treated as a geometrical parameter) and further, our model domain not only includes the position and orientation of the comb, but also the geometrical parameters. Further, by combining analytical models with regression we can take advantage of the existing literature on electrostatic comb models. The model is intended to be valid for multi-layer combs across a range of comb finger geometries, combined movement in vertical and lateral directions, and also include curling effects and fringe and corner capacitances. The model is also aimed at providing a energy-conserving description of the electrostatic comb actuator by fitting the derivative of the capacitance equation to numerically obtained force values. The model is intended for use in behavioral simulation of manufacturing variations in a CMOS-MEMS gyroscope and

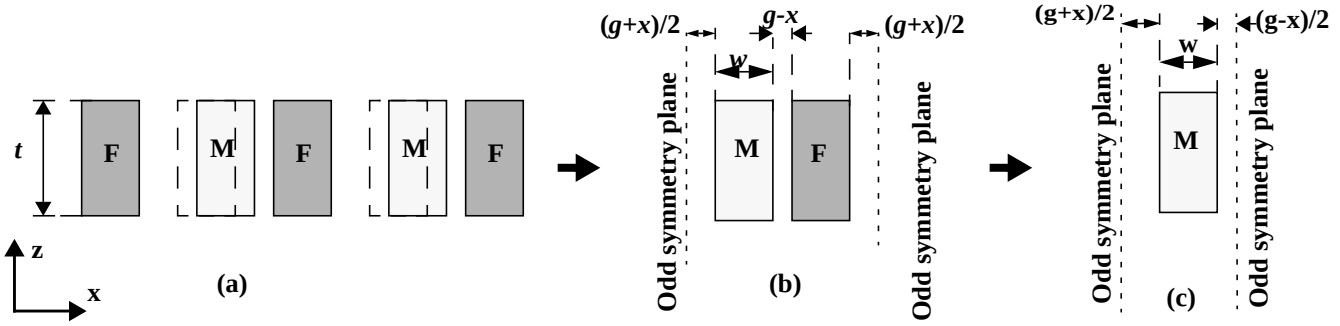

FIGURE 4. (a) Comb section showing 3 fixed fingers and 2 movable fingers displaced in the *x* direction from the nominal symmetrical position (shown with dotted lines). (b) Simplification by introduction of odd symmetry planes (c) Equivalent configuration with the fixed comb-fingers replaced by odd-symmetry plane placed midway between the rotor and stator fingers

other sensors as well.

In Section 2 we extend the library of existing analytical models for movement of the comb in the direction along the gap and briefly describe the analytical equations which form the core of the proposed model. Choice of design variables, variable screening, design of experiments for BEA are described in Section 3. Section 4 details the form of the model and the approach for combined modeling of capacitance and force. The regression results, accuracy of the fit and an application of the model to estimate manufacturing variation induced drive amplitude changes in a gyroscope are discussed in Section 5. Experimental verification is described in Section 6 and conclusions are presented in Section 7.

2 ANALYTICAL MODELS

In this section, we describe the analytical equations which will be used in the fitting formula. The cross-section of a comb with 3 fixed (F) and 2 movable (M) fingers is shown in Figure 4(a). The movable fingers are displaced to the right from the nominal position by *x*. The capacitance between the movable and fixed fingers can be written as a sum of two 2D capacitances, the parallel plate capacitance and the fringe capacitance. The parallel plate capacitance per unit length of overlap is given as:

$$c_p(t, g, x) = \varepsilon_0\left(\frac{t}{g+x} + \frac{t}{g-x}\right) \tag{1}$$

where, the parameters *t, g* and *x* are shown in Figure 4.

The derivation of the fringe capacitance is described below. Conformal mapping has been used in [6][7] to derive the capacitance for symmetric 2D cross-sections of different parts of the lateral comb. However, movement of one comb in the gap direction destroys the symmetry boundary conditions assumed in those derivations and renders the equations for fringe capacitance invalid. We present an alternative approach which is valid for movement along the gap direction. Assuming that there are a large number of fingers, we can use symmetry to simplify the geometry. By placing two odd symmetry planes we obtain the simplified configuration of Figure 4(b). Noting the presence of more symmetry, we arrive at Figure 4(c). The configuration of Figure 4(c) is basically a rectangular conductor placed asymmetrically between two ground planes and the conformal mapping for this case is given in [14]. This model is adapted to the configuration of Figure 4(a). From this model, the equations for the lateral force between the rotor and the stator comb-fingers are also derived. The model is verified by comparison with 2D FEA (Figure 5). The maximum error of 2% (which is at zero displacement for all gap values) is probably due to the finite number of fixed fingers (5) in the FEA. The small error suggests that the model is reasonably accurate even for 5 finger combs.

The total 2D capacitance per unit length per finger is given as:

$$C_{2D}(w, t, g, x) = c_p(t, g, x) + c_f(w, g, x) \tag{2}$$

where $c_f(w, g, x)$ is as shown in Figure 5. The capacitance thus derived is extended to 3D by multiplying C_{2D} with the overlap between the comb-fingers. The equation shown is valid for a single-layer structure and does not account for curling and corner capacitances. The next section describes the design of experiments for numerical analysis used to extend (2) to incorporate ver-

$$\alpha = \frac{w+g}{(g-x)/2}$$

$$\gamma = \frac{g+x}{g-x}$$

$$\beta = \frac{1}{2}\left(\alpha^2 - \gamma^2 - 1 + \sqrt{(\alpha^2 - \gamma^2 - 1)^2 - 4\gamma^2}\right);\ \delta = \frac{\beta^2}{\gamma^2}$$

$$C_l = \frac{\varepsilon_0}{\pi}\left(2\alpha\,\mathrm{atanh}\left(\sqrt{\frac{\beta+\delta}{\beta(1+\delta)}}\right) - 2\gamma\,\mathrm{atanh}\left(\frac{1}{\sqrt{\beta}}\right) - \ln\left(\frac{4\beta}{\beta-1}\right) + \ln(\delta)\right)$$

$$C_r = \frac{\varepsilon_0}{\pi}\left(\left(\frac{1}{\gamma}\right)\left(2\alpha\,\mathrm{atanh}\left(\sqrt{\frac{1+\beta}{\beta+\delta}}\right) + \gamma\ln\left(\frac{\beta-1}{4}\right) - 2\,\mathrm{atanh}\left(\frac{1}{\sqrt{\beta}}\right)\right) - \ln(\delta)\right)$$

$$c_f(w, g, x) = C_l + C_r$$

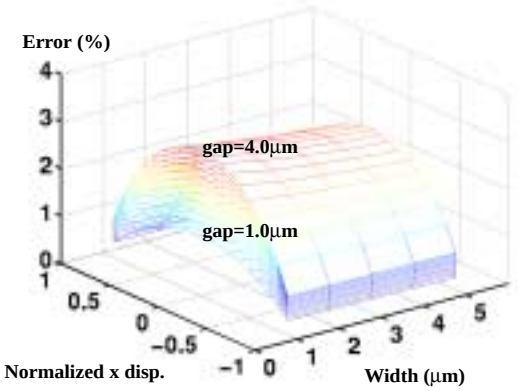

FIGURE 5. Comparison of analytical model adapted from [14] (the equation for edge fringe capacitance, $c_f(w, g, x)$, is shown on the left) and FEA for *x* displacement of the comb-finger cross-section shown in Figure 4. The *x* displacement was varied from 0 to 0.9 times the gap on either side. The model matches FEA to within 2%. The maximum error of 2% is probably because of the finite number (5) of comb-fingers in the simulation. The model underestimates the fringe capacitance on the end fingers because it assumes symmetry boundary conditions. It is seen that the error is maximum for maximum gap. This is because, the fringe capacitance of the end-fingers (and other fingers too) is significant when the gap is larger. At smaller gaps, the parallel plate capacitance begins to dominate.

tical movement, curling and 3D charge concentration effects.

3 DESIGN OF EXPERIMENTS AND SIMULATION

In this section the procedure for designing the experiments for BEA-based data collection to extend the 2D analytical model is described. Broadly the design of experiments process can be viewed in 4 steps: comb parameterization and variable selection, variable screening, choice of variable ranges and data collection.

The comb is parameterized into geometrical, position and orientation variables. The geometrical variables are: width (w), gap (g), overlap length (o_{lp}) and the number of fingers. The thickness of the comb depends on the composition of the multi-layer stack. For maximizing in-plane actuation force designers include all metal layers and the polysilicon layer. Therefore, we use the fixed comb cross-section containing all three metal layers and the polysilicon as shown in Figure 3. The three position (x, y, z) and three orientation variables (ϕ_x, ϕ_y, ϕ_z) correspond to the six degrees of freedom. Additionally, temperature (T) is also chosen as a variable because the curvature of the comb fingers is temperature dependent. Lateral combs are commonly used for actuation with amplitudes of the order of 5 μm. Since the force is independent of the finger length, it is usually tightly linked to the overlap length. Assuming a clearance of about 5 μm at maximum displacement, we arbitrarily set the finger length (l) to be dependent on the overlap length as:

$$l = o_{lp} + 10\mu m \tag{3}$$

The next step is to screen out variables which are known to have relatively small effect on the capacitance and force. Using data collected from initial runs varying each variable in isolation, it was decided that variables ϕ_y and ϕ_z can be kept at zero because of the small change in capacitance produced by them. The final set of variables used for the design of experiments are width, gap, overlap, positions x, y and z, orientation ϕ_x and the temperature T.

The values chosen for the variables are summarized in Table 1. The ranges for the width and the gap reflect commonly used values. The overlap length is limited to 20 μm since actuation combs are not likely to require greater than a few micrometers of movement, and when used for sensing, the capacitance change per unit length of displacement is independent of the overlap length. Larger number of fingers lead to larger number of panels in the boundary element mesh. Therefore, the number of fixed fingers was set to three to minimize the analysis time. Three fingers is the minimum number for which at least one finger on the movable part has symmetrical neighbors. Movements along the gap (x) direction are normally restricted to less than half the gap by limit stops or other means, however, we have chosen the maximum movement to be 0.8 times the gap in order that the

potential displacements are well within the validity range of the fitted model and also, in order to capture the highly non-linear capacitance change in the gap direction. The displacement along the length (y) was chosen to be 4 μm, with a view to keeping a clearance as well as a minimum overlap of at least twice the gap in order to avoid potentially non-linear regions which are undesirable for gyroscope actuation.

For maximizing sensitivity and actuation force, designers attempt to ensure maximum vertical overlap in the comb by using curl-matching techniques [8]. However, the resultant curl-matching is usually never perfect and the range chosen for z and ϕ_x variables is intended to capture curl mismatch in the combs. It should also be mentioned that $z = 0$ and $\phi_x = 0$ refer to the nominal curl-matched positions, from where z and ϕ_x are measured. At room temperature, the comb fingers are curled upward and the curling reduces as the temperature increases. The curvature of the comb fingers, computed using thermal multimorph theory presented in [15][16], is inversely proportional to the temperature. For a single finger the curvature ρ is related to the temperature T:

$$\frac{1}{\rho} \propto (T - T_0) \tag{4}$$

where, T_0 is the temperature where the finger will become flat and the constant of proportionality depends upon the composition of the finger and the material properties. We choose the temperature range of interest to be 50 K around the room temperature so that the corresponding range in curvature covers possible variations in finger composition and material properties from sensor to sensor. Also, it should be noted that by computing the curvatures of the finger we can operate independent of the temperature by directly feeding measured curvatures into the comb model rather than feeding temperature.

The variables and their bounds are summarized in Table 1. The experimental plan contains a total of 4374 runs. Note that the

TABLE 1. Variables and their bounds for capacitance BEA

VARIABLE TYPE	NAME (units)	Lower bound	Upper bound	Intermediate values
Geometry	w : width (μm)	2.0	4.0	3.0
	g : gap (μm)	1.5	2.5	2.0
	o_{lp} : overlap (μm)	10.0	20.0	-
Position	x (μm)	0	0.8 g	0.4 g
	y (μm)	-4.0	4.0	0.0
	z (μm)	-2.0	2.0	0.0
Orientation	$\phi_x(^\circ)$	-1.0	1.0	0.0
Temperature	temperature (K)	250	350	300
Constants	length (μm)	overlap + 10		
	numfingers	3		
	$\phi_y(^\circ)$	0		
	$\phi_z(^\circ)$	0		

comb response is symmetrical to positive and negative x position change, thus we need to collect data for positive x only.

AutoBEM software from Coventor [17] was used for BEA. A number of manual iterations with the BEA mesh led to an efficient template for the mesh which showed reduced simulation time with accuracy comparable to that obtained by adaptive refinement and iterative solution. Convergence of BEA using the template mesh was verified initially by splitting each element in the mesh into two and comparing the capacitance values obtained. A mesh generation program for electrostatic combs was implemented in C++. Figure 6 shows the boundary element mesh generated for a 10 finger curled comb. The curling and the curl-mismatch in the figure is exaggerated to aid visualization. Also, the actual refinement used for solution leads to very small elements and is not shown in the figure.

Force computation using BEA did not converge even with a mesh which was more than four times as fine as the mesh required for capacitance convergence (and therefore about 4 times slower). Therefore, only capacitance convergence was

obtained for the first set of 4374 runs. Force convergence was attempted on a smaller subset of 1458 runs, in which ϕ_x was also kept constant at 0. However, convergence testing revealed that the force values were not accurate, though the capacitance values obtained were more accurate than those in the first set of 4374 runs. Therefore, we resorted to numerical differentiation of the well-converged capacitance values in the second set of 1458 runs to obtain the forces (F_y and F_z), in the y and z directions respectively, for 972 intermediate points. We obtained F_y values at y=- 2 and +2 μm, from capacitance values at y=-4, 0 and 4 μm and F_z values at z= -1 and +1 μm from capacitance values at z=-2, 0 and 2 μm. This method could not be used for computing the force (F_x) in the x direction because the capacitance change in the x direction is highly non-linear and therefore, required closely spaced points for precise computation of force. Therefore a separate set of 162 runs, as summarized in Table 2 was

TABLE 2. Variables and their bounds for F_x runs. All other variables are set to their mean values.

VARIABLE TYPE	NAME (units)	Lower bound	Upper bound	Intermediate values
Geometry	w : width (μm)	2.0	4.0	-
	g : gap (μm)	1.5	2.5	-
	o_{lp} : overlap (μm)	10.0	20.0	-
Position	x (μm)	0.4 g - 0.1	0.4 g + 0.1	0.4 g
	y (μm)	-4.0	4.0	-
	z (μm)	-2.0	2.0	0.0
Temperature	temperature (K)	250	350	-

designed to compute F_x at 54 points. Note that because of the rapid change in capacitance with x, three capacitance values were used to compute each force value.

4 MODELING METHODOLOGY

We first describe the form of the equation for the capacitance model. Following this we present an approach for combined modeling of capacitance and force so that the force models can use the same fitting equation and coefficients as the capacitance.

4.1 Capacitance Modeling

We use the two analytical equations described in Section 2 as the core of the model and weight them by polynomial functions

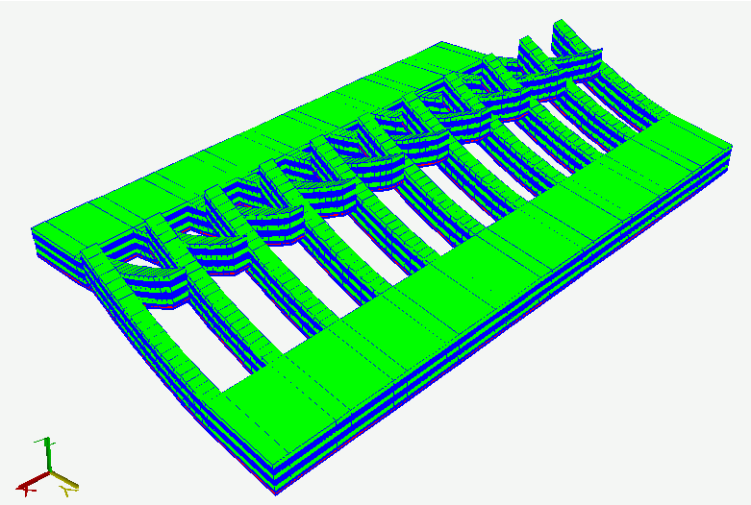

FIGURE 6. Boundary-element mesh for a 10 finger vertically curled lateral comb with all CMOS layers.

of variables. The fitting function used for linear regression is of the form:

$$C = c_1(\ldots)f_1(\ldots) + c_2(\ldots)f_2(\ldots) + c_2(\ldots)f_3(\ldots) \tag{5}$$

where,
t is the total thickness of the multi-layer comb finger which is held constant
$(\ldots)$ indicates function of all the variables in Table 1
c_1, c_2 and c_3 are capacitance functions of the design variables given as:
$c_1(\ldots) = (o_{lp} + y)c_p(t, g, x)$ is the 2D parallel-plate capacitance given in (1)
$c_2(\ldots) = (o_{lp} + y)c_f(w, g, x)$ is the 2D fringe capacitance as given by the equations in Figure 5
$c_3(\ldots) = 1$
$f_1(\ldots)$, $f_2(\ldots)$, $f_3(\ldots)$ are the polynomial weighting functions. $f_3(\ldots)$ corresponds to that part of the capacitance which is not due to the parallel plate or the analytical fringe capacitance.

Let us assume that the number of polynomial terms in f_1, f_2 and f_3 are k_1, k_2 and k_3 respectively and that all the terms are sequentially numbered from 1 to k, where $k = k_1 + k_2 + k_3$.The polynomial weighting function can be written as:

$$f_i(\ldots) = \sum_{j=(k_1+\ldots+k_{i-1})}^{(k_1+\ldots+k_i)} r_j(w^{a_{j1}} g^{a_{j2}} o_{lp}^{a_{j3}} \rho^{a_{j4}} x^{a_{j5}} y^{a_{j6}} z^{a_{j7}} \phi_x^{a_{j8}}) \tag{6}$$

where, r_j are the coefficients and $a_{j1}, \ldots, a_{j8}$ are the powers to which the respective variables are raised to in the j th polynomial term. Note that the unity term as well as negative indices can also be included in the polynomial representation. The coefficients of the polynomial terms will be obtained by regression. For the above regression model, there are k predictor terms which are products of the three capacitance functions and the polynomial terms associated with that function. Evaluating each of k predictor terms at the n data points where we have obtained capacitance values we can form the model matrix:

$$[C]_{nX1} = [p_1 \; p_2 \; \ldots]_{nXk} \begin{bmatrix} r_1 \\ r_2 \\ \ldots \end{bmatrix}_{kX1} \tag{7}$$

where,
$[C]$ is the vector of capacitance values corresponding to *n* runs in the experimental plan.
p_j is the *j*th predictor vector. There are *k* predictor vectors of size $nX1$ corresponding to the *n* settings of the variables.
r_j is the regression coefficient associated with the *j*th predictor vector.

4.2 Combined Capacitance-Force Modeling

The force produced by an electrostatic actuator, assuming constant voltage, in a generalized direction ξ is given as:

$$F_\xi = \frac{1}{2}\left(\frac{dC}{d\xi}\right)V^2 \tag{8}$$

Therefore, we can write the regression model for the force (assuming unit voltage) in the direction ξ as:

$$\left[F_\xi\right]_{m_\xi X1} = \frac{1}{2}\left[\frac{dp_1}{d\xi} \; \frac{dp_2}{d\xi} \; \ldots\right]_{m_\xi Xk} \begin{bmatrix} r_1 \\ r_2 \\ \ldots \end{bmatrix}_{kX1} \tag{9}$$

where, m_ξ is the total number of data points for which we have the force values in the direction ξ. To obtain regression coef-

ficients which produce accurate fitted values for both force and capacitance simultaneously, we combine (7) and (9) into a common regression model:

$$\begin{bmatrix} C \\ F_x \\ F_y \\ F_z \end{bmatrix}_{(n+m_x+m_y+m_z)X1} = \frac{1}{2}\begin{bmatrix} 2p_1 & 2p_2 & \cdots \\ \frac{dp_1}{dx} & \frac{dp_2}{dx} & \cdots \\ \frac{dp_1}{dy} & \frac{dp_2}{dy} & \cdots \\ \frac{dp_1}{dz} & \frac{dp_2}{dz} & \cdots \end{bmatrix}_{(n+m_x+m_y+m_z)Xk} \begin{bmatrix} r_1 \\ r_2 \\ \cdots \end{bmatrix}_{kX1} \tag{10}$$

In the above equation n, m_x, m_y, m_z correspond to the number of data points at which we have capacitance F_x, F_y and F_z respectively. As per the experimental plan described in Section 3, we have $n = 4374$, $m_x = 54$, $m_y = 972$ and $m_z = 972$. Since the capacitance and force obtained may differ in their relative magnitudes, weights may be necessary to scale the residual errors corresponding to each point so that points with smaller absolute values of capacitance or force but relatively large percentage errors are not ignored by the regression.

5 RESULTS

The number of BEA and the type of data obtained from them is summarized in Table 3. The times shown are for analyses

TABLE 3. Summary of BEA runs for different quantities

Quantity	Number of values obtained	Total number of BEA runs	No. of BE panels (approx.)	Memory required per run (MB)	Time taken per run (minutes)
Capacitance	n=4374	4374	22000	230	5
F_x	m_x=54	162	90000	850	24
F_y	m_y=972	1458	90000	850	24
F_z	m_z=972	1458	90000	850	24

run on one CPU of a 450 MHz Sun Ultra-80 workstation. Multi-processor usage leads to corresponding speed up. Note that the F_x values were computed using three closely spaced capacitance data points while the F_y and F_z values used a common set of 1458 capacitance values to compute derivatives at 972 points. The runs used to obtain capacitance values for computing forces used higher mesh refinement, and therefore, required higher memory and CPU times.

The model matrix shown in (10) was constructed in the S-Plus [18] environment. Polynomial terms and fitting weights were introduced by iterative manual analysis of residual errors. The reusability of the proposed model justifies the time investment in this procedure. The final comb model has 106 coefficients and fits the capacitance data to within 3% as shown in Figure 7 for 4374 points. It should be noted that there are only a few points which lie outside the 2%band. The fitted values of force in all three directions match the values obtained by numerical differentiation to about 10%,as seen in Figure 8, Figure 9 and Figure 10. The error tends to be high for point where the absolute values of force is small (i.e., the difference in the capacitances used to compute the derivative is small). This may be because the difference is close to the precision limit of the numerical capacitance values.

The comb model was implemented in Verilog-A, an Analog Hardware Description Language, as part of the NODAS framework [12] and was used in simulation of a CMOS-MEMS gyroscope [3]. In order to demonstrate the applicability of the model to study manufacturing variations two sets of simulations were done. An extended study of manufacturing variations on the gyroscope is available in [19]. The output parameter of interest in these simulations was the drive amplitude of the gyroscope. Microgyroscopes are known to have significant Zero Rate Output (ZRO) and the ZRO is closely related to the drive amplitude. In the first set of simulations the vertical offset between the movable and fixed portions of the actuation comb in the gyroscope was varied from 0 to 1 μm. As seen in Figure 11, a 1 μm offset leads to about 4% decrease in the drive amplitude. Temperature

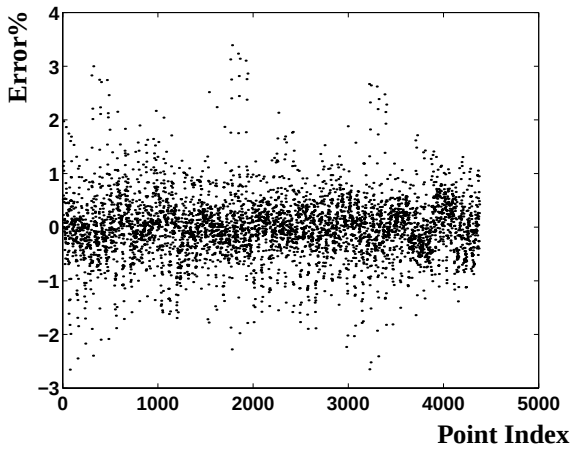

FIGURE 7. Error in % between model and numerical data for 4374 capacitance points. The error is almost within 3%

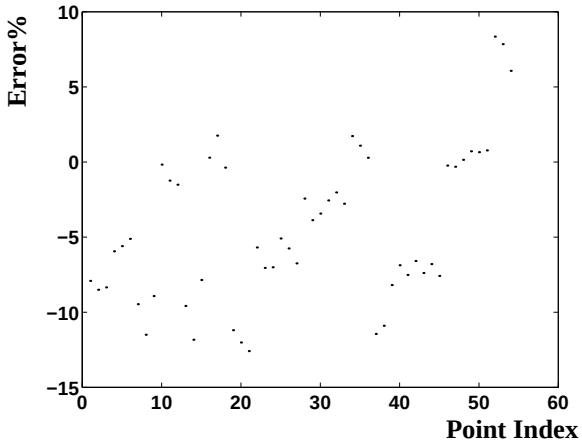

FIGURE 8. Error in % between model and F_x from numerical derivative of capacitance w.r.t x

changes can lead to change in vertical overlap and thus cause drive amplitude and ZRO drifts. In the second set of simulations, we varied the gap in the comb actuator to estimate drive amplitude change due to overetch-induced gap variation across different gyroscopes. A 5% increase in the comb gap leads to about 4% reduction in the drive amplitude as shown in Figure 12.

6 EXPERIMENTAL VERIFICATION

Test structures for measurement of capacitance changes have been fabricated (Figure 13). They consist of two structures identical to that shown in Figure 13, which are connected in series as shown in Figure 14. The capacitance change is sensed and amplified using a chopper-stabilized amplifier circuit [8], which has a known gain set by ratioed resistors. Current passing through resistors R_1 and R_2 heats up the capacitors C_1 and C_2 respectively and changes their values because of the change in curvature of the fingers and increased vertical overlap between the fixed and movable fingers. The profile of the entire structure is obtained using interferometry for different values of heating current. For the same values of heating current the output voltage of the amplifier is also noted. The output voltage is given as:

$$\frac{V_o}{V_m} = \frac{C_1 - C_2}{C_1 + C_2 + C_p} A \tag{11}$$

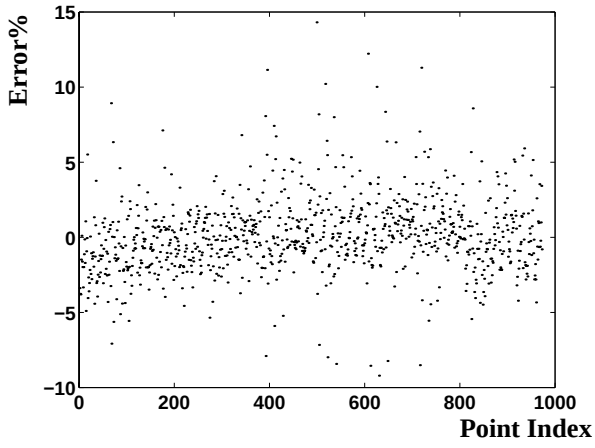

FIGURE 9. Error in % between model and F_y obtained from numerical derivative of capacitance w.r.t. y.

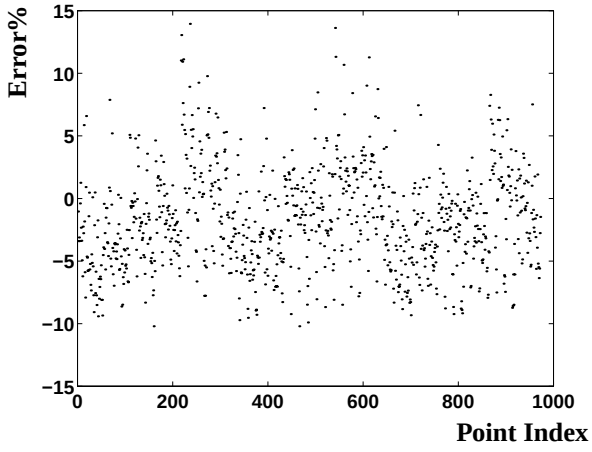

FIGURE 10. Error in % between model and F_z obtained from numerical derivative of capacitance w.r.t. z.

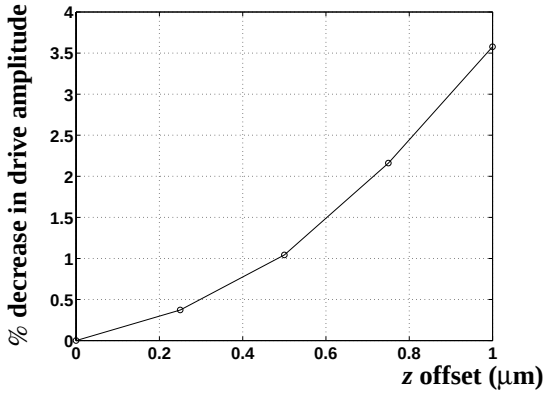

FIGURE 11. Drive amplitude variation of a gyroscope with change in vertical overlap between the movable and fixed portions of the comb actuator.

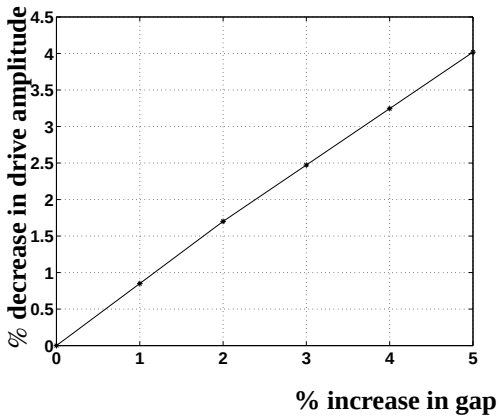

FIGURE 12. Drive amplitude variation across different gyroscopes due to overetch-induced gap variation. The slope of the above line is less than 1 because of the fringe capacitance which changes slower with the gap than parallel plate capacitance

where, V_m is the fractional modulation voltage (i.e., $V_m = D(V_{mp} - V_{mn})$, where D is the duty cycle of the chopping waveform) and A is the overall gain.

The comparison of the capacitance change predicted by the model and the measured capacitance change is shown in Figure 15. There are two sets of curves corresponding to voltage applied to the two heaters. In both cases the values of capacitance change simulated using the model developed match the experimentally measured values to about 10% at higher heater voltages. At lower heater voltages the larger error is probably due to the limited accuracy of the profile of the comb fingers. All the fingers in the comb do not have the same vertical offset, because of curling of the movable frame. Therefore, the measurements are made on the fingers which approximately represent the mean vertical offset. This can also potentially contribute to the total error. Further, larger gaps due to overetching can also lead to lower measured capacitance change.

7 CONCLUSIONS

A modeling methodology which combines the ease of use of analytical equations and the higher accuracy of numerical methods has been demonstrated for a CMOS-MEMS comb. The methodology automatically results in an energy conserving model for the comb actuator. BEA is used to obtain capacitance values for a designed set of 4374 runs and force values for a reduced

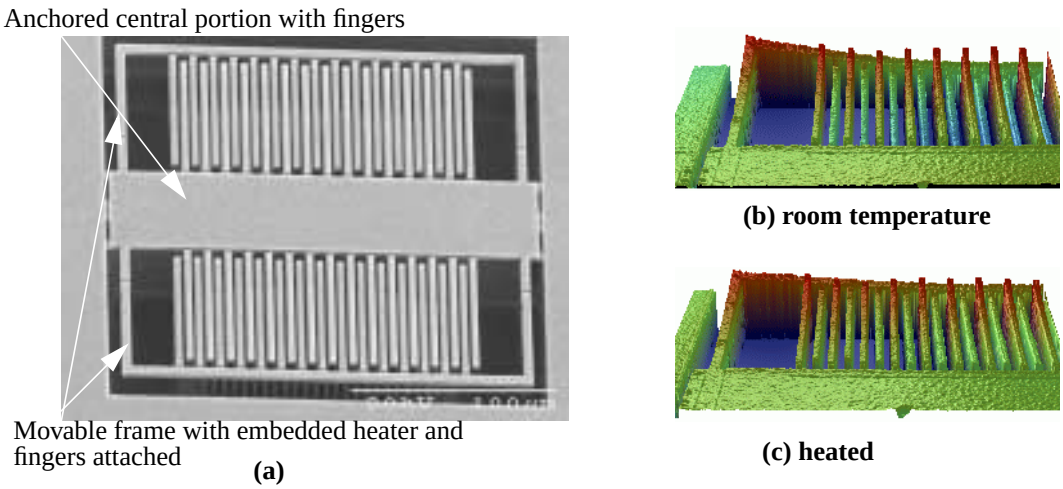

FIGURE 13. (a) SEM of capacitance test structure with in-built heaters. The curling can be changed by changing the current passing through the polysilicon wires which pass through the outer frame of the structure. Interferometry images of a quarter of the structure at (b) room temperature and (c) heated are also shown.

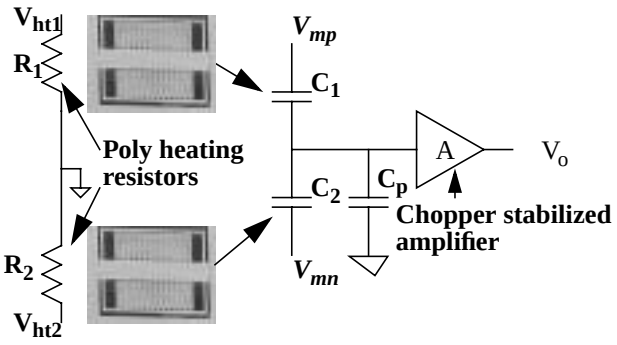

FIGURE 14. Capacitance change measurement schematic shown with heating resistors for each structure. C_p is the parasitic capacitor whose value is obtained using layout extraction.

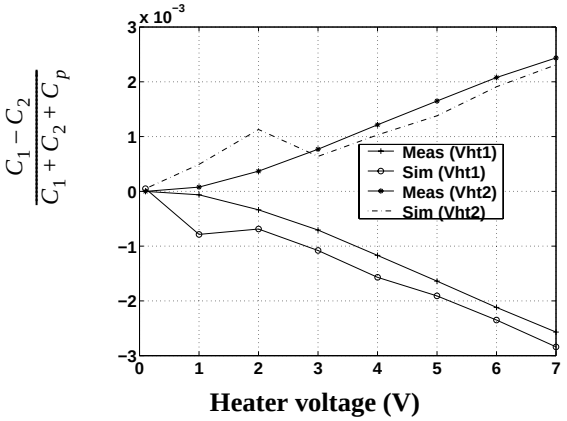

FIGURE 15. Comparison of measured and predicted capacitance change. The two sets of measured data correspond to the voltage applied to each of the two resistors, with 0.1 V applied to the other resistor.

subset of these runs. The comb model fits the BEA capacitance data to within 2%(there are very few points which fall outside this error range) and take into account the corner capacitances as well as curling of the multi-layer comb fingers. Convergence of force requires higher mesh refinement for BEA. Therefore, BEA for a large number of runs to obtain converged force values was found to be infeasible. Numerical derivatives of a reduced subset of the capacitance runs were used to obtain force values. The fitted values of force match the numerically computed values match to within 10%,though a large fraction of the points match to within 5%. The models obtained are used to predict the capacitance change of thermally actuated combs and they match measured capacitance changes to about 10%. The comb model has been implemented in a behavioral simulation framework and its applicability for simulating manufacturing variations has been demonstrated.

ACKNOWLEDGMENTS

The authors thank Xu Zhu for post-processing and releasing the test structures. This research effort is sponsored by the MARCO Center for Circuits, Systems and Software, the Defence Advanced Research Projects Agency (DARPA) and U. S. Air Force Research Laboratory, under agreement number and F30602-99-2-0545 and in part by the National Science Foundation award CCR-9901171.

REFERENCES

[1] W. C. Tang. T. -C. H. Nguyen, M. W. Judy, and R. T. Howe, “Electrostatic-comb Drive of Lateral Polysilicon Resonators,” *Proc. 5th Int. Conf. Solid-State Sensors and Actuators (Transducers ‘89)*, Montreux, vol. 2, pp. 328-331, June 25-30 1989

[2] M. Lemkin and B. E. Boser, “A Micromachined Fully Differential Lateral Accelerometer,” *Proc. Custom Integrated Circuits Conf. (CICC ‘96)*, San Diego, 315-318, May 5-8, 1996

[3] H. Luo, G. K. Fedder, L. R. Carley, “An Elastically Gimbaled Z-Axis CMOS-MEMS Gyroscope,” *Proc. Int. Sym. Smart Structures & Microsystems*, Hong Kong, Oct. 19-21, 2000

[4] G. K. Fedder, S. Santhanam, M. L. Reed, S. C. Eagle, D. F. Guillou, M. S.-C. Lu, and L. R. Carley, “Laminated High-Aspect-Ratio Microstructures in a Conventional CMOS Process,” *Sensors and Actuators A*, vol. A57, no. 2, pp. 103-110, 1996

[5] S. D. Senturia, “CAD Challenges for Microsensors, Microactuators, and Microsystems,” *Proc. IEEE*, vol. 86, pp. 1611-1626, Aug. 1998

[6] W. A. Johnson and L. K. Warne, “Electrophysics of Micromechanical Comb Actuators,” *J. Microelectromechanical Systems*, pp. 49-59, vol. 4, no. 1, March 1995

[7] G. Lorenz, *Network Simulation of Microelectromechanical Systems*, Ph. D. Thesis, University of Bremen, December 1999

[8] H. Lakdawala and G. K. Fedder, “Temperature Control of CMOS micromachined sensors,” *IEEE MEMS Workshop*, Las Vegas, NV, 2002

[9] H. Xie, L. Erdmann, Q. Jing, and G. K.Fedder, “Simulation and Characterization of a CMOS Z-axis Microactuator with Electrostatic Comb Drives,” *Proc. Int. Conf. Modeling and Simulation of Microsystems (MSM ‘00)*, San Diego, CA, March 27-29, 2000

[10] J. Wu and L. R. Carley, “Table-based Numerical Macromodeling for MEMS Devices,” *Proc. Int. Conf. Modeling and Simulation of Microsystems (MSM ‘01)*, 68-71, Hilton Head Island, South Carolina, March 19-21, 2001

[11] M. S-C. Lu and G. K. Fedder, “Parameterized Electrostatic Gap Models for Structured Design of Microelectromechanical Systems”, *Proc. Int. Conf. Modeling and Simulation of Microsystems (MSM ‘99)*, 280-283, San Juan, Puerto Rico, April 19-21, 1999

[12] G. K. Fedder, Q. Jing, “A Hierarchical Circuit-level Design Methodology for Microelectromechanical Systems”, *IEEE Transactions on Circuits and Systems II*, vol. 46, no. 10, pp 1309-1315, 1999

[13] L. D. Gabbay, J. E. Mehner, and S. D. Senturia, “Computer-Aided Generation of Nonlinear Reduced-order Dynamic Macromodels-I: Non-stress-stiffened case,” *J. Microelectromechanical Systems*, vol. 9, no. 2, pp. 262-269, June 2000

[14] W. H. Chang, “Analytic IC Metal-line Capacitance Formulas”, *IEEE Trans. Microwave Theory Techniques*, pp. 608-611, September 1979

[15] H. Lakdawala, G. K. Fedder, “Analysis of Temperature-Dependent Residual Stress Gradients in CMOS Micromachined Structures”, *Proc. 10th Int. Conf. Solid-State Sensors and Actuators (Transducers ‘99)*, 526-259, Sendai, Japan, June 1999

[16] S. Iyer, H. Lakdawala, G. K. Fedder and T. Mukherjee, “Macromodeling Temperature-Dependent Curl in CMOS Micromachined Beams”, *Proc. Int. Conf. Modeling and Simulation of Microsystems (MSM ‘01)*, 88-91, Hilton Head Island, South Carolina, March 19-21, 2001

[17] http://www.coventor.com

[18] http://www.splus.com

[19] S. V. Iyer and T. Mukherjee, “Simulation of Manufacturing Variations in a Z-axis CMOS-MEMS Gyroscope,”, to appear in *Proc. Int. Conf. Modeling and Simulation of Microsystems (MSM ‘02)*, Puerto Rico, April 22-24, 2002